

Proper motions of spectrally selected structures in the HH 83 outflow^{★ ★★ ★★}

T.A. Movsessian¹, T.Yu. Magakian¹, and A.V. Moiseev²

¹ Byurakan Astrophysical Observatory, 0213 Aragatzotn prov., Armenia
e-mail: tigmov@bao.sci.am, tigmag@sci.am

² Special Astrophysical Observatory, N.Arkhiz, Karachaevo-Cherkesia, 369167 Russia
e-mail: moisav@sao.ru

Received ...; / Accepted ...

ABSTRACT

Context. We continue our program of investigation of the proper motions of spectrally separated structures in the Herbig-Haro outflows with the aid of Fabry-Perot scanning interferometry. This work mainly focuses on the physical nature of various structures in the jets.

Aims. The aim of the present study is to measure the proper motions of the previously discovered kinematically separated structures in the working surface of the HH 83 collimated outflow.

Methods. We used observations from two epochs separated by 15 years, which were performed on the 6m telescope with Fabry-Perot scanning interferometer. We obtained images corresponding to different radial velocities for the two separate epochs, and used them to measure proper motions.

Results. In the course of our data analysis, we discovered a counter bow-shock of HH 83 flow with positive radial velocity, which makes this flow a relatively symmetric bipolar system. The second epoch observations confirm that the working surface of the flow is split into two structures with an exceptionally large (250 km s⁻¹) difference in radial velocity. The proper motions of these structures are almost equal, which suggests that they are physically connected. The asymmetry of the bow shock and the turning of proper motion vectors suggests a collision between the outflow and a dense cloud. The profile of the H α line for the directly invisible infrared source HH 83 IRS, obtained by integration of the data within the reflection nebula, suggests it to be of P Cyg type with a broad absorption component characteristic of the FU Ori-like objects. If this object underwent an FU Ori type outburst, which created the HH 83 working surfaces, its eruption took place about 1500 years ago according to the kinematical age of the outflow.

Key words. ISM: jets and outflows – ISM: individual objects: HH 83 – Stars: pre-main sequence – Stars: individual: HH 83 IRS (IRAS 05311–0631)

1. Introduction

High proper motions (PMs) of Herbig-Haro (HH) objects were discovered about 40 years ago. The orientation of the PM vectors of HH objects, which represent shocked excitation regions, revealed the bipolar nature of high velocity flows responsible for their formation (Herbig & Jones 1981; Jones & Herbig 1982). Further discoveries of highly collimated jets from young stellar objects indicated that HH objects are the brightest parts of these flows (Reipurth et al. 1986, 1993); in subsequent studies these were named HH jets and flows.

Further investigations of HH flows revealed their complex morphology. In particular, high- and low-excitation zones, which were separated by ground-based and Hubble Space Telescope (HST) narrow band imagery (Reipurth et al. 1997; Hartigan et al. 2011) as well as by long-slit spectroscopy (Heathcote & Reipurth 1992; Reipurth et al. 1997; Hartigan et al. 2011), were revealed in terminal working surfaces (WSs) and inside certain knots in the jets. The full morphology

and kinematics of these structures can be understood using methods of spectral imaging (Hartigan et al. 2000; Movsessian et al. 2000; Movsessian et al. 2009).

Briefly, inside the terminal WSs, which is the common term for the regions where supersonic flow slams directly into the undisturbed ambient medium (Reipurth & Bally 2001), as well as in the internal WSs of jets, two principal shock structures form: a “reverse shock”, which decelerates the supersonic flow, and a “forward shock”, which accelerates the ambient material with which the flow collides (e.g. Hartigan 1989).

In addition, various other shocked structures, such as deflection shocks, evacuated cavities, intersecting shock waves, Mach stems, clumps, and sheets, can form in HH flows (Hartigan et al. 2011). The study of such structures can help us to obtain a global understanding of the processes taking place inside the collimated outflows. Proper motion measurements of already separated kinematical structures are of great importance for the discovery and analysis of all the above types of shocked structures.

The subject of the present work is the HH 83 system. Its wiggling knotty jet emerges from IRAS 05311–0631 source. This source, being deeply embedded in a molecular cloud, is not visible in the optical range, but it illuminates the edges of a conical cavity formed by the outflow (Reipurth 1989). At the distance of 105'' from the beginning of the jet, a bow shock structure was

* This work is based on observations conducted with the 6m telescope of the Special Astrophysical Observatory of the Russian Academy of Sciences.

** The channel movie is available at...

*** Reduced datacubes (FITS files) are only available at the CDS via anonymous ftp to...

found, which is visible in $H\alpha$ emission, but not in $[S\ II]$ IIR (Reipurth 1989).

Our previous observations of HH 83 with scanning Fabry Perot interferometer (FPI) revealed separated structures with very different radial velocities in the terminal WS (more than 2 km s^{-1}), and confirmed the steady increase in velocity along the jet depending on the distance from the source (Movsessian et al. 2009). Furthermore, unusual wave-like variations in the radial velocity of the jet as a function of distance from the source are also visible in the values of full width at half maximum (FWHM) of emission lines.

The present investigation was motivated by our two-epoch study of the HL Tau jet, where observations from 2001 and 2017 were used to estimate the PM of spectrally separated structures in the jet. This method, applied to HH jets for the first time to the best of our knowledge, reveals that the structural components inside the jet, which can be divided into components of low- and high-radial velocity, have, nevertheless, very similar values of PM (Movsessian et al. 2012). This important result was also confirmed for the components inside the FS Tau B jet system (Movsessian et al. 2019). The HH 83 system represents the next suitable object for second epoch spectra-imagery observations, especially in view of the discovery of two separated kinematical structures in its WS. However, HH 83 is a much more distant object than the Taurus dark cloud. Taking this into account we decided to increase the time between the two epochs to up to 15 years.

2. Observations and data reduction

Observations were carried out in the prime focus of the 6m telescope of the Special Astrophysical Observatory of the Russian Academy of Sciences in two epochs: 10 February 2002 and 2 February 2017, in good atmospheric conditions (seeing was about $1''$). We used a FPI placed in the collimated beam of the Spectral Camera with Optical Reducer for Photometric and Interferometric Observation (SCORPIO) (Afanasiev & Moiseev 2005) and SCORPIO-2 (Afanasiev & Moiseev 2011) multi-mode focal reducers in 2002 and 2017, respectively. The capabilities of these devices in scanning FPI observational mode are presented in Moiseev (2002, 2015). A description of the first epoch observations was presented by Movsessian et al. (2009).

During the second epoch of observations, the detector was a EEV 40-90 $2 \times 4.5\text{K}$ CCD array. The observations were performed with 4×4 pixel binning, and so 512×512 pixel images were obtained for each spectral channel. The field of view was $6.1'$ with a scale of $0.72''$ per pixel. The second epoch of observations provided deeper images and of higher spectral resolution.

The scanning interferometer was ICOS FPI operating in the 751st order of interference at the $H\alpha$ wavelength, providing a spectral resolution of $\text{FWHM} \approx 0.4\text{\AA}$ (or $\approx 20\text{ km s}^{-1}$) for a range of $\Delta\lambda = 8.7\text{\AA}$ (or $\approx 390\text{ km s}^{-1}$) free from order overlapping. The number of spectral channels was 40 and the size of a single channel was $\Delta\lambda \approx 0.22\text{\AA}$ ($\approx 10\text{ km s}^{-1}$). In both epochs an interference filter with $\text{FWHM} \approx 15\text{\AA}$ centered on the $H\alpha$ line was used for pre-monochromatization.

We reduced our interferometric observations using the software developed at the SAO (Moiseev 2002; Moiseev & Egorov 2008; Moiseev 2015) and the ADHOC software package¹. After

¹ The ADHOC software package was developed by J. Boulestex (Marseille Observatory) and is publicly available on the internet.

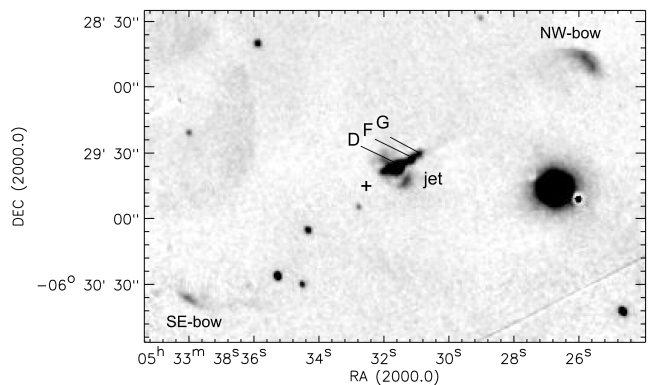


Fig. 1. Monochromatic image in $H\alpha$ line of the HH 83 outflow system, which consists of a narrow jet (main knots are marked) and two WSs in NW and SE directions from the source (seen only in the infrared range and marked here by a cross).

primary data reduction, subtraction of night-sky lines, and wavelength calibration, the observational material was organised into “data cubes”. We applied optimal data filtering, which included Gaussian smoothing over the spectral coordinate with $\text{FWHM} = 1.5$ channels and spatial smoothing using a two-dimensional Gaussian with $\text{FWHM} = 2\text{--}3$ pixels. The FPIs used in the two epochs of observations had different spectral resolutions. Therefore, the rebinned data cubes were created for both epochs to bring them into the same velocity steps. This allows a better comparison of morphological details that have the same radial velocities. All radial velocities presented in this paper are heliocentric.

Using these data cubes, we spectrally separated the details with a different radial velocity in the outflow system. Proper motions were then measured for the selected structures using observations in both epochs. For the PM estimation, we used a method of optimal offset computation for two images by means of cross-correlation (this is the ‘IDL’ procedure by F. Varosi and included in the IDL astronomy library²).

3. Results

During the observations, the field of view of the SCORPIO focal reducer covered the entire HH 83 outflow system including the jet, the WS, and the reflection nebula around the source (which actually represents the illuminated cavity walls). Below we discuss all these parts of HH 83 separately and compare the observations of 2002 and 2017.

Due to the higher quantum efficiency (QE) of both the new detector and the whole optical system, the data from the second epoch have a better S/N in comparison with those of the first epoch. Figure 1 shows the integrated $H\alpha$ image of the HH 83 system built using the second epoch observations. The main details are marked.

3.1. The terminal working surfaces, their proper motions, and kinematical structures

Besides the already known WS (further denoted as NW-bow) which lies at a distance of about $2'$ from the source, our image clearly shows a second bow-shape structure in the opposite direction from the source, not described previously (Fig. 1). This structure lies on the axis of the outflow system at nearly

² <https://idlastro.gsfc.nasa.gov/>

the same distance from the source as the main NW-bow. After re-examining the first epoch data, we found faint traces of this second bow-shaped structure in the same place. In contrast with the NW-bow, this second bow shock has positive radial velocity. It undoubtedly represents the terminal WS of the counter flow (further SE-bow), confirming the bipolar and symmetric nature of this outflow system.

In the first paper (Movsessian et al. 2009) we mentioned the significant asymmetry of the NW-bow as well as the trend of the decreasing radial velocity from the apex toward the end of the wing of the bow shape structure. Using new observations, we built a velocity channel map of low-velocity structures in the NW-bow of the HH 83 outflow system (Fig. 2). This channel map confirms that the low-velocity component of the NW-bow shows noticeable differences in morphology depending on the radial velocity. At relatively high velocities, it has a more or less symmetric shape, and at lower velocities it becomes more and more asymmetric.

As mentioned above, our previous data demonstrated that the NW-bow in the HH 83 system is divided into two distinct components, which are spectrally and spatially well separated (see Fig. 6 in Movsessian et al. 2009). After Gaussian fitting of both components of $H\alpha$ emission we restored images of these components for each observational epoch. Using these images we measured the PMs of high- and low-radial-velocity structures in the NW-bow.

The results of our PM measurements are presented in Fig. 3. In particular, the PM vectors for both the low- and high-radial-velocity structures of the NW-bow of the HH 83 flow are shown in the inset. Both structural components can be seen to have very similar values of PM, despite the large difference in radial velocity. We also estimated the distance between these structures during the second epoch observations and we find this distance to be the same as for the first epoch (1000 AU). This is additional evidence of their equal PM values. We discuss this result in more detail in the following section.

In Fig. 3 we also show the PM vectors for the three brightest knots in the HH 83 jet, and for the separated structures in the NW-bow and the SE-bow, that is for the counter bow shock. It is worth mentioning that this second bow shock has nearly the same range of radial velocities (in absolute values) as the NW-bow, but, unlike the latter, it does not show either a spectral or a spatial inner separation. In any case, we were able to measure the PM of this structure, even though it was significantly fainter in the first epoch data.

The numerical results are given in Table 1 where we present the distances for each structure measured from the source position, values of tangential velocities (computed for the distance of 450 pc), position angles (PAs) of PM vectors, radial velocities, and calculated absolute spatial velocities.

3.2. Proper motions of the knots in the jet

We measured the PMs of several bright knots in the HH 83 jet, namely knots D, G, and F (according to the nomenclature of Reipurth 1989). These knots also show high values of PM (see Table 1) similar to those of high- and low-velocity structures in the terminal WS. It should be noted, however, that although the geometric axis of the jet coincides with that of the NW-bow, the position angles of the PM vectors of the jet knots significantly differ from those of the structures in the NW-bow: they are turned in the northern direction for about 14 degrees. The spatial velocities of the knots, calculated from their radial and tangential velocities, increase along with the distance from the

source. The same trend is observed in their radial velocities (see Table 1). We discuss this effect in the following section.

The knots in the HH 83 jet do not demonstrate a distinct division into high- and low-radial-velocity components; consequently it was impossible to reveal the morphological structures with different radial velocities inside them.

3.3. Radial velocities of the system in general

The radial velocities estimated from the second epoch FP observations are in good agreement with those of the first epoch. Figure 4 shows the position velocity diagram and the integrated $H\alpha$ image of the HH 83 outflow. New observations with higher spectral resolution confirm an increase in the negative radial velocity with distance from the source, and also confirm the remarkable split in radial velocity inside the terminal NW-bow. The counter bow-shock (SE-bow) has high positive velocity over a significant range (FWHM $\sim 150 \text{ km s}^{-1}$). The whole system represents a bipolar collimated flow with a full size of about 0.48 pc.

To compare the observations of both epochs, we built the distributions of radial velocities and FWHM of $H\alpha$ emission along the HH 83 jet itself (Fig. 5). These show a good match to the previous data shown in Figs. 3 and 4 of Movsessian et al. (2009) and confirm the existence of wave-like variations in the general trend of these parameters. We discussed these variations in this latter paper, but the new data provide higher spectral resolution and S/N. The prominent steep drops between knots A and D, as well as between D and F, are clearly seen in Fig. 5. In these regions the steep increase in FWHM is observed as well; though in general we see a constant decrease in FWHM values along the jet, as in other cases.

3.4. The reflection nebula

Observations show that the HH 83 jet is propagating through the evacuated conical cavity formed by wide-angle wind from the deeply embedded infrared source (Reipurth et al. 2000). The walls of this cavity are illuminated by light from this source. In the optical range, these walls form two reflection lobes around the narrow jet. In the high-resolution infrared images (Reipurth et al. 2000), several spiral or helical arms can be seen on the cone walls, somewhat similar to the structures observed in GM 3-12 (RNO 124) nebula (Movsessian et al. 2004). On the PanSTARRS i band image (see Fig. 6, lower panel) these two lobes are connected by a bar-like structure, which probably represents one of the above-mentioned arms. On the restored $H\alpha$ image (Fig. 6, upper panel) these details are almost invisible, which confirms their reflection nature.

The above-mentioned high quality of the new data allows an attempt to obtain the profile of the $H\alpha$ line in the spectrum of the central star through the scattered light of the source deeply embedded in the dark cloud. To study the profile of the $H\alpha$ line in the reflected light we used spectral imaging, which allows the data to be summarized and the total line profiles to be constructed for any selected area. To avoid contamination from the jet radiation and to deal with pure continual (i.e., reflected) light, we integrated profiles from the two side lobes only, excluding the bar-like structure, which is superimposed on the D knot of the jet. The resulting integrated $H\alpha$ profile is presented in the right panel of Fig. 6. This profile has strong and wide ($\sim 300 \text{ km s}^{-1}$) blueshifted absorption with a weak emission component near the zero radial velocity. We assume that this profile corresponds to the invisible IR source.

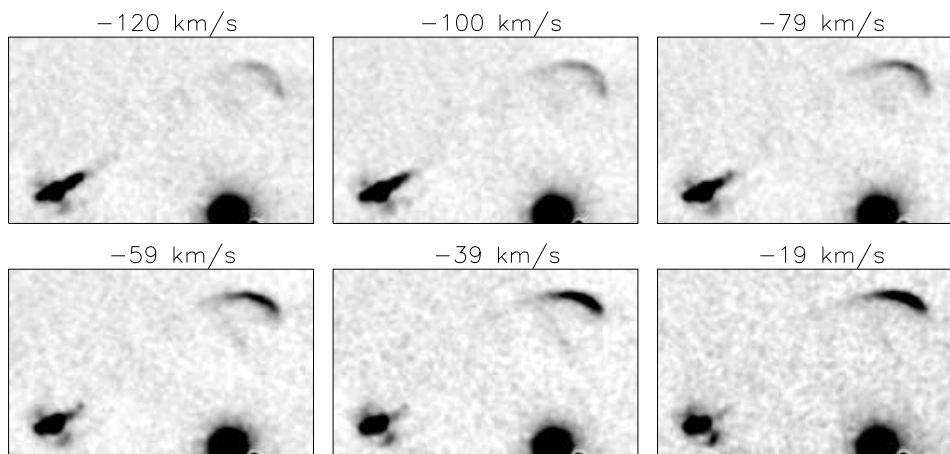


Fig. 2. Velocity channel map of HH 83 outflow system showing morphology variations of the low velocity structure in NW bow

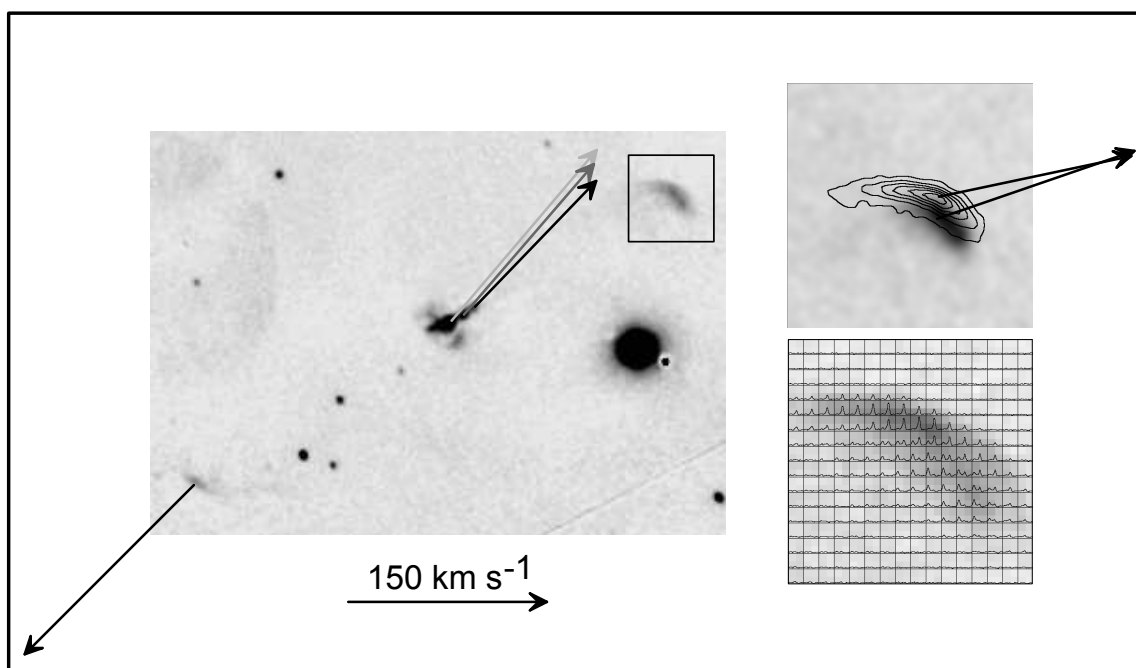


Fig. 3. $H\alpha$ image of the HH 83 outflow system integrated over all velocity channels, with superposed PM vectors for the jet knots and the counterflow (left panel). The bottom right panel shows the grid of $H\alpha$ profiles in the NW bow. The significant split of profiles for the high- and low-velocity components is obvious (the absolute velocity values decrease to the right). Separate images of the low-velocity (contours) and high-velocity components (grey scale) based on the intensities obtained by the Gaussian fitting of the profiles of both components are presented in the top right panel. The corresponding PM vectors also are shown.

4. Discussion

4.1. Working surface

Comparing the inner structures in the WS of HH 83 and in the knots in the HL Tau jet, in both cases we find two emission structures with very different radial velocities. However, in the HL Tau jet these structures differ not only in their radial velocities but also in excitation, while in parts of the HH 83 WS the excitation level does not change, and these structures are visible mainly in $H\alpha$ (Reipurth 1989).

The radial velocities of these two emission structures differ by more than 250 km s^{-1} . This is a unique case: for example, two velocity components in the WS of HH 111 differ by about 60 km s^{-1} only (Reipurth et al. 1997) and the two components in the HL Tau jet differ by about 100 km s^{-1} . This large difference in speed cannot be explained by the existence of two separate

outbursts, which formed two bow-shape structures with strongly different radial velocities, because in this case the high-velocity structure will catch up to the low-velocity one in 15 years; in addition, our new observations reveal that the PMs of these structures are the same.

Therefore, we conclude that we observe physically connected structures in the terminal WS of HH 83 that can be designated a reverse shock and a forward shock. The observed large difference in the radial velocities of these structures can form in very extreme conditions. For example, in the case of the HL Tau jet, the bright low-velocity structures in front of the high-velocity knots appear only in the region where the collisional interaction between the jet and wide outflow from XZ Tau is taking place (Movsessian et al. 2007).

The asymmetry of the bow-shock as well as the turning of its PM vectors compared to those of the jet knots are further

Table 1. Proper motions and radial velocities of knots in the HH 83 outflow

Knot	Distance (arcsec)	V_{tan}^a (km s^{-1})	PA (deg)	V_r (km s^{-1})	V_{abs} (km s^{-1})
D	13.5	120 ± 30	310	-130	177
F	19.3	142 ± 35	327	-140	200
G	27.8	135 ± 40	319	-165	213
WS <i>high vel</i>	117.0	160 ± 23	282	-312	351
WS <i>low vel</i>	119.4	145 ± 30	277	-50	153^b
counter bow	96	180 ± 45	135	+180	255

Notes. ^(a) Tangential velocities correspond to a distance of 450 pc for the flow ^(b) The value of this velocity is discussed below in Sect. 4.1

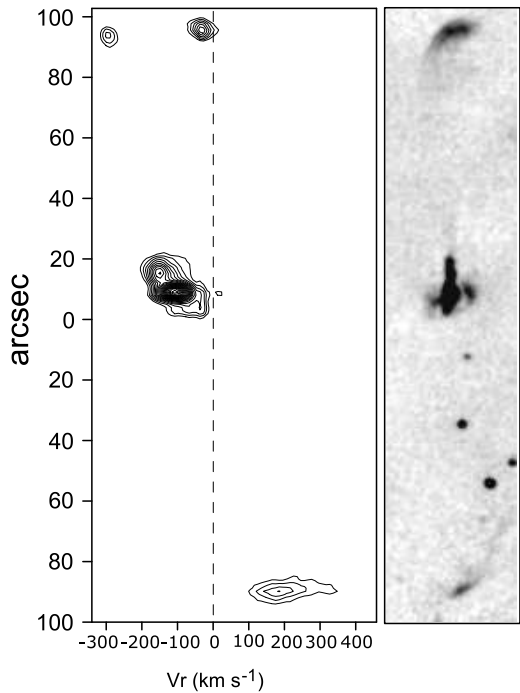


Fig. 4. Position-velocity diagram along the full length of the HH 83 system, including both WSs and the jet. The NW WS clearly separates into two distinct structures.

indications of the encounter between the jet and the dense cloud core. A well-known example of a similar jet collision with dense cloud is HH 110 (Reipurth et al. 1996; López et al. 2010).

Here we observe the bow with increased brightness of the wing, probably formed by an oblique collision. Analysis of the morphology of the bow in various radial velocities using a velocity channel map (Fig. 2) shows that the bow is more symmetric at higher velocities, and the apex of the bow can be seen in the channels corresponding to radial velocities near $100\text{--}120 \text{ km s}^{-1}$. However, this value is still much lower than that for the reverse shock region.

Taking into account the simple bow-shock and Mach disk model of Hartigan (1989), such a velocity difference could occur when the ratio of the density of the ambient medium to that of the jet is near 100, and with a jet velocity of more than 300 km s^{-1} .

If our conclusion is correct and the high-velocity structure in the WS indeed represents a reverse shock, then we detect emission of the decelerated flow matter; the ratio of pattern speed to flow speed in this structure will, by definition, be equal to one. On the contrary, for the forward shock, which represents

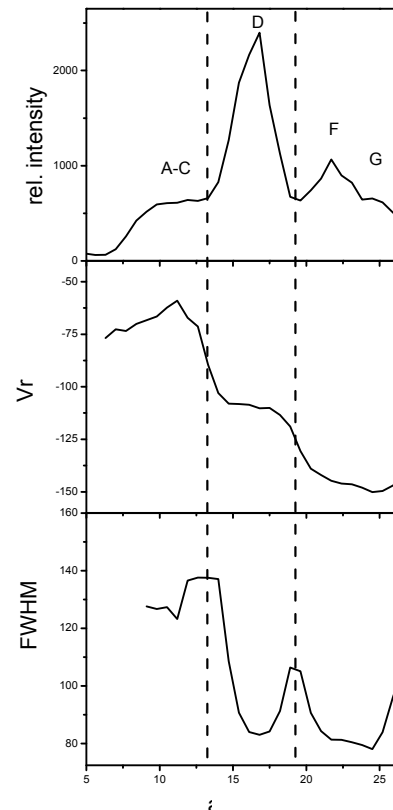


Fig. 5. Plots of the intensity, radial velocity, and FWHM of the $H\alpha$ emission in the HH 83 jet versus position. The abrupt rise in FWHM after $25''$ is associated with the $H\alpha$ emission. The S/N.

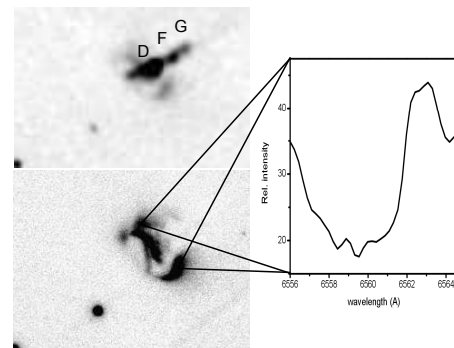


Fig. 6. Integrated profile of the $H\alpha$ line in the reflected light of the source of HH 83. The left side shows an enlarged image of the central part of HH 83 system in $H\alpha$ emission (the integrated FP image from 2017, upper panel) and in i band (PanSTARRS survey, lower panel).

accelerated matter from the ambient medium, this ratio will be much higher because of the lower radial velocities of the emitting particles. Based on this, we calculated the spatial velocities of the flow structures, presented in the Table 1; one should keep in mind that only the values for the reverse shock represent the real flow velocity. In this way, it is possible to compute the inclination angle between the line of sight and the jet, which we find to be close to 27 degrees. Using all these values, one can estimate the kinematical age of the outflow to be about 1500 years.

In general, the structures with different radial velocities in the terminal WS of HH 83 outflow are similar to the inner structures in the HL Tau jet. But there are certain differences. The high-velocity structure in the WS of HH 83 is not as compact as in the case of the HL Tau jet and represents an extended object consisting of several condensations. We think that this is caused by fragmentation of the jet matter during its collision with a dense cloud core. Presumably, it forms a common forward shock region, which we see as a narrow bow-shape structure.

4.2. The jet

Unfortunately the spatial resolution of our observations is not sufficient to resolve various velocity structures in the knots of the HH 83 jet. As mentioned above, the data obtained in 2017 confirm the increase in absolute radial velocity values with distance from the source. The obtained PMs of the knots also indicate a small increase in tangential velocities. Using both velocity components, we calculated the spatial velocities for the three knots; they show the same behavior. This result rules out an explanation of the increase in radial velocities by bending of the jet. The wave-like oscillations superposed on the general increase in velocity can be the result of the quasi-periodical variations in the rate of matter ejection. The FWHM along the jet peaks between the knots. However, a thorough analysis of the profiles shows that this effect (in certain places even a split of emission is detected) could be the result of overlapping neighboring knots caused by seeing effects. On the other hand, high values of FWHM can be seen in the starting part of the jet, near the knots A-C. As these knots are located in the zone where the outflow enters the cavity in the dark cloud, such a large range of velocities could perhaps be related to the interaction of the matter of the outflow with the cavity walls.

4.3. The source IRAS 05311–0631

The analysis of the reflected spectrum of the HH 83 source shows that it has a P Cyg-type $H\alpha$ line profile with a wide, almost rectangular absorption and a faint secondary blueshifted peak. Such profiles are likely to be formed in a strong wind with optical depth sufficient to produce the deep blueshifted absorption component (e.g., Muzerolle et al. 2011); they are highly typical of FU Ori-type eruptive stars; on the other hand, only a few T Tauri stars show such well-developed P Cygni profiles at $H\alpha$ line. The blue edge of the absorption trough indicates wind velocities of up to 300 km s^{-1} . This value is nearly the same as the velocity of the powerful wind that emanates from FU Orionis (e.g., Herbig et al. 2003).

The detection of faint CO absorption bands at $2.3 \mu\text{m}$ by Davis et al. (2011) can be considered as a further argument in favor of the FU Ori-type nature of IRAS 05311–0631. Such absorption bands, though usually more strong, are typical for FUors (e.g., Reipurth & Aspin 1997).

On the other hand, FU Ori phenomena in nearly all cases are associated with HH outflows (Audard et al. 2014). Moreover, the spacing of the structural details in some HH outflows corresponds to the statistical estimates of the supposed recurrence of the FUor events (Herbig et al. 2003). In this case, the bright WS of the HH 83 flow could be the result of an FU Ori-type outburst, which took place about 1500 years ago judging by the kinematical age of the outflow.

5. Conclusion

This work is a continuation of a series of investigations of PMs of spectrally separated structures in collimated outflows from young stars based on observations with a scanning Fabry-Perot interferometer conducted in different epochs. Taking into account the discussions above in conjunction with previously obtained results, we draw several conclusions, and make some further suggestions as outlined below.

1. During our observations we discovered a second WS in the opposite direction to the previously known WS, which indicates the bipolar nature of the HH 83 outflow system.
2. Our estimation of the tangential velocities of the two previously discovered kinematically distinct structures in the NW-bow indicates similar values.
3. We are inclined to assume that the structures of different velocity in the NW-bow represent two principal shocks, namely reverse and forward shocks, as in the case of the internal WSs of the HL Tau jet.
4. The asymmetry of the NW-bow and the very large difference in radial velocities for the two separate structures lead us to conclude that the flow collides with dense cloud in this region.
5. The increase in the spatial velocity of the knots in the HH 83 jet once again shows that the behavior of radial velocities cannot be explained by jet bending.
6. Our analysis of the $H\alpha$ line in the reflection nebula allows us to define the nature of the source of outflow system—which is deeply embedded in a molecular cloud and is not visible in the optical range—as an FU Ori-type object that underwent outburst about 1500 years ago (taking into account the kinematical age of the NW WS).

We hope that this work will be useful for the development of new theoretical models of collimated outflows and of their interaction with the interstellar medium. The confirmation of HH 83 IRS (IRAS 05311–0631) as an FU Ori-like object is important because of the very small number of known representatives of this class of eruptive stars. Further study of this object will help to gain a better understanding of these phenomena.

Acknowledgements. Authors thank referee for the helpful comments. This work was supported by the Science Committee of RA, in the frames of the research project 18T-1C329. Observations with the SAO RAS telescopes are supported by the Ministry of Science and Higher Education of the Russian Federation (including agreement No05.619.21.0016, project ID RFMEFI61919X0016). The Pan-STARRS1 Surveys (PS1) have been made possible through contributions of the Institute for Astronomy, the University of Hawaii, the Pan-STARRS Project Office, the Max-Planck Society and its participating institutes, the Max Planck Institute for Astronomy, Heidelberg and the Max Planck Institute for Extraterrestrial Physics, Garching, The Johns Hopkins University, Durham University, the University of Edinburgh, Queen's University Belfast, the Harvard-Smithsonian Center for Astrophysics, the Las Cumbres Observatory Global Telescope Network Incorporated, the National Central University of Taiwan, the Space Telescope Science Institute, the National Aeronautics and Space Administration under Grant No. NNX08AR22G issued through the Planetary Science Division of the NASA Science Mission Directorate, the National Science Foundation under Grant No. AST-1238877, the University of Maryland, and Eotvos Lorand University (ELTE).

References

- Afanasiev V.L., & Moiseev A.V., 2005, *Astronomy Letters*, 31, 194
- Afanasiev V.L., & Moiseev A.V., 2011, *Baltic Astronomy*, 20, 363
- Audard, M., Ábrahám, P., Dunham, M.M. et al. 2014, in *Protostars and Planets VI*, Univ. Arizona Press, eds. H. Beuther et al., 387
- Davis, C.J., Cervantes, B., Nisini, B. et al., 2011, *A&A*, 528, A3
- Hartigan, P., 1989, *ApJ*, 339, 987
- Hartigan, P., Morse, J., Palunas, P., et al. 2000, *AJ*, 119, 1872
- Hartigan, P., Frank, A., Foster, J. M., et al. 2011, *ApJ*, 736, 29
- Heathcote, S. & Reipurth, B. 1992, *AJ*, 104, 2193
- Herbig, G. H., & Jones, B. F. 1981, *AJ*, 86, 1232
- Herbig, G. H., Petrov, P. P., & Dummmler, R. 2003, *ApJ*, 595, 384
- Jones, B. F., & Herbig, G. H. 1982, *AJ*, 87, 1223
- López, R., García-Lorenzo, B., Sánchez, S. F., et al. 2010, *MNRAS*, 406, 2193
- Moiseev, A.V., 2002, *Bull. Spec. Astrophys. Obs.*, 54, 74
- Moiseev, A.V., 2015, *Bull. Spec. Astrophys. Obs.*, 70, 94
- Moiseev, A.V., & Egorov, O.V. 2008, *Bull. Spec. Astrophys. Obs.*, 63, 181
- Movsessian, T. A., Magakian, T. Y., Amram, P., et al. 2000, *A&A*, 364, 293
- Movsessian, T. A., Magakian, T. Y., Boulesteix, J., Amram, P. 2004, *A&A*, 413, 203
- Movsessian, T. A., Magakian, T. Y., Bally, J., et al. 2007, *A&A*, 470, 605
- Movsessian, T. A., Magakian, T. Yu., Moiseev, A. V., & Smith, M. D., 2009, *A&A*, 508, 773
- Movsessian, T. A., Magakian, T. Y., & Moiseev, A. V. 2012, *A&A*, 541, A16
- Movsessian, T. A., Magakian, T. Y., Burenkov, A. N. 2019, *A&A*, 827, A94.
- Muzerolle, J., Calvet, N., Hartmann, L. 2001, *ApJ*, 550, 944.
- Reipurth, B., Bally, J., Graham, J. A., et al. 1986, *A&A*, 164, 51
- Reipurth, B., 1989, *A&A* 220, 249
- Reipurth, B. 1989, *European Southern Observatory Conference and Workshop Proceedings*, 247
- Reipurth, B., Raga, A. C., & Heathcote, S. 1996, *A&A*, 311, 989
- Reipurth, B., Raga, A. C., & Heathcote, S. 1992, *ApJ*, 392, 145
- Reipurth, B., & Heathcote, S. 1992, *A&A*, 257, 693
- Reipurth, B., Heathcote, S., Roth, M., et al. 1993, *ApJ*, 408, L49
- Reipurth, B., Hartigan, P., Heathcote, S., Morse, J., & Bally, J. 1997, *AJ*, 114, 757
- Reipurth, B., Hartigan, P., Heathcote, S., et al. 1997, *AJ*, 114, 757
- Reipurth, B., & Aspin, C.A. 1997, *AJ*, 114, 2700
- Reipurth, B., Yu, K. C., Heathcote, S., et al. 2000, *AJ*, 120, 1449
- Reipurth, B., & Bally, J. 2001, *ARA&A*, 39, 403